On the numerical evaluation of elastostatic fields in locally isotropic two-dimensional composites

Helsing, Johan; Greengard, Leslie

Published in:
Journal of the Mechanics and Physics of Solids

DOI:
10.1016/S0022-5096(97)00041-0

1998

On the numerical evaluation of elastostatic fields in locally isotropic two-dimensional composites

Leslie Greengard* Johan Helsing†

March 10, 1997

Abstract

We present a fast algorithm for the calculation of elastostatic fields in locally isotropic composites. The method uses an integral equation approach due to Sherman, combined with the fast multipole method and an adaptive quadrature technique. Accurate solutions can be obtained with inclusions of arbitrary shape at a cost roughly proportional to the number of points needed to resolve the interface. Large-scale problems, with hundreds of thousands of interface points can be solved using modest computational resources.

1 Introduction

An important problem in planar elasticity concerns the calculation of elastostatic fields in composite materials consisting of locally isotropic inclusions in a uniform background. Important quantities which can be obtained from the elastic field include the effective elastic moduli of the composite as well as pointwise values of the stress, strain and displacement fields. A variety of numerical methods have been used for such problems including finite element methods (Garboczi and Day 1995; Lukkassen, Persson and Wall 1995), boundary element methods (Achenbach and Zhu 1990; Eischen and Torquato 1993), collocation methods (Jou, Leo and Lowengrub 1995), and spring-grid models (Chen, Thorpe and Davis 1995). Methods applicable to special geometries, such as ellipsoids and half-planes, include algebraic transformation methods (Honein and Herrmann 1990) and Fourier methods (McPhedran and Movchan 1994; Helsing 1995). Finite difference schemes can also be used, as well complex variable methods and the equivalent inclusion method (Mura 1987).

Despite the many available options, however, accurate numerical solutions are difficult to obtain due to issues of storage, speed, quadrature and the imposition of periodic boundary

*Courant Institute of Mathematical Sciences, New York University, New York, New York 10012. The work of this author was supported by the Applied Mathematical Sciences Program of the U.S. Department of Energy under Contract DEFGO288ER25053 and by a NSF Presidential Young Investigator Award

†Courant Institute of Mathematical Sciences, New York University, New York, New York 10012. The work of this author was supported by the Applied Mathematical Sciences Program of the U.S. Department of Energy under Contract DEFGO288ER25053 and by NFR, TFR, and the Knut and Alice Wallenberg Foundation under TFR contract 96-977. Present address: Department of Solid Mechanics, Royal Institute of Technology, SE-100 44 Stockholm, Sweden

conditions. We have chosen to concentrate on developing an approach due originally to Sherman (1959), who constructed an elegant complex variable method based on the Goursat or Kolosov-Muskhelishvili potentials. In particular, he showed that it is possible to rewrite the elastostatic equations as a singular integral equation for a complex-valued density. As far as we know, Sherman's equation has not been used in practice, although Theocaris and Ioakimidis (1977) have suggested the use of a closely related approach.

In this paper, we present a simple version of the Sherman equation, a high-order quadrature method, and a fast algorithm for solving the finite-dimensional linear system which results from discretization. This algorithm relies on conjugate-gradient type iterative methods such as GMRES (Saad and Schultz 1986) or BCG (Lanczos 1952; Fletcher 1975), together with fast multipole acceleration (Rokhlin 1985; Greengard and Rokhlin 1987; Carrier *et al.* 1988). The net cost is roughly proportional to the number of points on the interface. Related schemes have previously been developed for electrostatic interface problems (Greengard and Moura 1994; Helsing 1996) and Stokes flow (Greengard *et al.* 1996).

The next section describes the Sherman equation, while section 3 provides an extension of the equation to periodic problems and a collection of formulae for extracting effective moduli. We briefly discuss some numerical issues in section 4, and demonstrate the performance of the method in section 5.

2 The Sherman Equation

Let U denote the Airy stress function for a piecewise isotropic two-dimensional material. Since U satisfies the biharmonic equation (in each subdomain), it can be represented as

$$U = \Re\mathrm{e}\left\{\bar{z}\phi + \chi\right\}, \tag{1}$$

where ϕ and χ are analytic functions of the complex variable z and $\Re\mathrm{e}\{f\}$ denotes the real part of the function f. For a thorough discussion of the complex variable approach to elasticity problems, see (Muskhelishvili 1953; Parton and Perlin 1981). For our purposes, it is sufficient to observe that the displacement (u, v) satisfies

$$u + iv = \left(\frac{1}{2\mu} + \frac{1}{\kappa}\right)\phi - \frac{1}{2\mu}\left(z\overline{\phi'} + \overline{\psi}\right), \tag{2}$$

where $\psi = \chi'$, κ is the two-dimensional bulk modulus, and μ is the two-dimensional shear modulus. The integral of the traction (t_x, t_y) along a curve $\Gamma(s)$ can be obtained from the relation

$$\int_{\Gamma(s_0)}^{\Gamma(s)} (t_x + it_y)\mathrm{d}s = -\Big|_{s_0}^{s} i\left(\phi + z\overline{\phi'} + \overline{\psi}\right), \tag{3}$$

where s denotes arclength. Differentiation of the expression (2) along the tangent to a curve Γ with normal (n_x, n_y) yields

$$\frac{\mathrm{d}}{\mathrm{d}s}(u + iv) = i\left(\frac{1}{2\mu} + \frac{1}{\kappa}\right)\Phi n - \frac{i}{2\mu}\left(\overline{\Phi}n - z\overline{\Phi'}\bar{n} - \overline{\Psi}\bar{n}\right), \tag{4}$$

where $n = n_x + in_y$, $\Phi = \phi'$, and $\Psi = \psi'$. Finally, differentiation of the expression (3) along the tangent yields

$$t_x + it_y = \Phi n + \overline{\Phi}n - z\overline{\Phi'}\bar{n} - \overline{\Psi}\bar{n}. \tag{5}$$

Consider now a two-component material consisting of an infinite medium D_0 with elastic moduli κ_1 and μ_1 which surrounds a finite number M of inclusions with elastic moduli κ_2 and μ_2. We will refer to the infinite medium as *filler*. We denote the inclusions by D_j, $j = 1, \ldots, M$, the interface between D_0 and D_j by Γ_j, and the union of all interfaces by $\Gamma = \sum_{j=1}^{M} \Gamma_j$. We would like to compute the displacement, stress, and strain fields in the material subject to three different imposed average displacements, namely $d_{\rm I} = (x, 0)$, $d_{\rm II} = (0, y)$, and $d_{\rm III} = (y, x)$. Since the equations of elasticity are satisfied in each domain, it remains only to solve the interface problem, which consists of enforcing the continuity of traction and displacement across inclusion/filler boundaries.

The first option, suggested by Sherman (1959), is to work with eq. (2) and eq. (3) and to represent the lower-case potentials ϕ and ψ in the form

$$\phi(z) = \frac{1}{2\pi i} \int_\Gamma \frac{\omega(\tau) \mathrm{d}\tau}{\tau - z} + \alpha z, \tag{6}$$

and

$$\psi(z) = \frac{1}{2\pi i} \int_\Gamma \frac{\omega(\tau) \mathrm{d}\bar{\tau} - \overline{\omega(\tau)} \mathrm{d}\tau}{\tau - z} - \frac{1}{2\pi i} \int_\Gamma \frac{\bar{\tau} \omega(\tau) \mathrm{d}\tau}{(\tau - z)^2} + \beta z, \tag{7}$$

where $\omega(z)$ is an unknown density.

Remark 2.1 The functions αz and βz in eqs. (6) and (7) represent the forcing terms in our formulation. The two constants α and β take the values $\kappa_1/2$ and $-\mu_1$ for imposed average displacement $d_{\rm I}$, the values $\kappa_1/2$ and μ_1 for displacement $d_{\rm II}$, and the values 0 and $2i\mu_1$ for displacement $d_{\rm III}$. Thus, α can always be assumed to be real, while β is either real or a pure imaginary number. While the displacements are clearly unbounded at infinity, the stresses are not. If we let N_1 and N_2 denote the principal stresses at infinity, and let θ denote the angle made by the direction of N_1 with respect to the x-axis, then it is straightforward to show that $\alpha = \frac{1}{4}(N_1 + N_2)$ and $\beta = -\frac{1}{2}(N_1 - N_2)e^{-2i\theta}$.

Remark 2.2 Sherman (1959) considered a slightly different situation, where the filler phase D_0 is finite, and is subject to some specified displacement on its boundary ∂D_0. The differences between these two problems are minor, and the formulation presented above is more readily extended to the periodic case.

Once ϕ is assumed to take the form (6), the expression (7) for ψ enforces the continuity across the interface of the integral of traction. The requirement that the displacement be continuous across the interface leads, from eq. (2), to the integral equation

$$\frac{1}{2}\left(\frac{1}{\mu_2} + \frac{1}{\kappa_2} + \frac{1}{\mu_1} + \frac{1}{\kappa_1}\right)\omega(z) + \left(\frac{1}{\kappa_2} - \frac{1}{\kappa_1}\right) M_1\omega(z) + \left(\frac{1}{2\mu_2} - \frac{1}{2\mu_1}\right) M_2\omega(z) =$$

$$- \left(\frac{1}{\kappa_2} - \frac{1}{\kappa_1}\right)\alpha z + \left(\frac{1}{2\mu_2} - \frac{1}{2\mu_1}\right)\bar{\beta}\bar{z}, \tag{8}$$

where M_1 and M_2 are integral operators given by

$$M_1\omega(z) = \frac{1}{2\pi i} \int_\Gamma \frac{\omega(\tau) \mathrm{d}\tau}{\tau - z}, \tag{9}$$

and

$$M_2\omega(z) = \frac{1}{2\pi i}\int_\Gamma \omega(\tau)\mathrm{d}\left[\log\frac{\tau-z}{\bar\tau-\bar z}\right] + \frac{1}{2\pi i}\int_\Gamma \overline{\omega(\tau)}\mathrm{d}\left[\frac{\tau-z}{\bar\tau-\bar z}\right]$$

$$= \frac{1}{2\pi i}\left[\int_\Gamma \frac{\omega(\tau)\mathrm{d}\tau}{\tau-z} - \int_\Gamma \frac{\omega(\tau)\mathrm{d}\bar\tau}{\bar\tau-\bar z} + \int_\Gamma \frac{\overline{\omega(\tau)}\mathrm{d}\tau}{\bar\tau-\bar z} - \int_\Gamma \frac{(\tau-z)\overline{\omega(\tau)}\mathrm{d}\bar\tau}{(\bar\tau-\bar z)^2}\right]. \tag{10}$$

Despite appearances, the operator M_2 is smooth, while the operator M_1 is to be interpreted in the Cauchy principal value sense (see section 4). The equation (8) is simpler than Sherman's original formulation, but mathematically equivalent.

A second way to solve the inclusion problem, suggested by Theocaris and Ioakimidis (1977), is to work with eqs. (4) and (5) and to represent the upper-case potentials Φ and Ψ as Cauchy-type integrals:

$$\Phi(z) = \frac{1}{2\pi i}\int_\Gamma \frac{\Omega(\tau)\mathrm{d}\tau}{\tau-z} + \alpha, \tag{11}$$

and

$$\Psi(z) = -\frac{1}{2\pi i}\int_\Gamma \frac{\overline{\Omega(\tau)}\mathrm{d}\bar\tau}{\tau-z} - \frac{1}{2\pi i}\int_\Gamma \frac{\bar\tau\Omega(\tau)\mathrm{d}\tau}{(\tau-z)^2} + \beta. \tag{12}$$

With this choice, the continuity of traction condition is automatically satisfied. The requirement of a continuous displacement leads, via eq. (4), to an integral equation for $\Omega(z)$:

$$\frac{1}{2}\left(\frac{1}{\mu_2}+\frac{1}{\kappa_2}+\frac{1}{\mu_1}+\frac{1}{\kappa_1}\right)\Omega(z) + \left(\frac{1}{\kappa_2}-\frac{1}{\kappa_1}\right)M_1\Omega(z) + \left(\frac{1}{2\mu_2}-\frac{1}{2\mu_1}\right)M_3\Omega(z) =$$

$$-\left(\frac{1}{\kappa_2}-\frac{1}{\kappa_1}\right)\alpha - \left(\frac{1}{2\mu_2}-\frac{1}{2\mu_1}\right)\frac{\bar n}{n}\bar\beta, \tag{13}$$

where, M_1 is defined in eq. (9), and the operator M_3 is defined by

$$M_3\Omega(z) = \frac{1}{2\pi i}\left[\int_\Gamma \frac{\Omega(\tau)\mathrm{d}\tau}{\tau-z} + \frac{\bar n}{n}\int_\Gamma \frac{\Omega(\tau)\mathrm{d}\tau}{\bar\tau-\bar z} + \int_\Gamma \frac{\overline{\Omega(\tau)}\mathrm{d}\bar\tau}{\bar\tau-\bar z} + \frac{\bar n}{n}\int_\Gamma \frac{(\tau-z)\overline{\Omega(\tau)}\mathrm{d}\bar\tau}{(\bar\tau-\bar z)^2}\right].$$

We will work with eq. (8) rather than eq. (13) for two reasons: first, the operator M_2 is simpler than M_3, and second, the density $\omega(z)$ is smoother than the density $\Omega(z)$. The former is, in fact, the integral of the latter.

3 Periodic Boundary Conditions and Effective Moduli

In order to study bulk properties of composites at finite volume (area) fraction, we consider a periodic structure which tiles the entire plane. To simplify the ensuing discussion, we limit our attention to square arrays (Fig. 1). We denote the unit cell in this structure by $D_0 = [-1/2, 1/2)\times[-1/2, 1/2)$. Given M inclusions per unit cell (D_1,...,D_M), we denote the area fraction they occupy by p_2.

There are a number of ways of imposing periodic boundary conditions. One of the most natural, as well as one of the oldest, is the method of images (Rayleigh 1892). Let $\boldsymbol{Z}^2$ denote the set of lattice points in the plane with integer coordinates,

$$\boldsymbol{Z}^2 = \{k_1 + ik_2 \,|\, k_1, k_2 \in \boldsymbol{Z}\}.$$

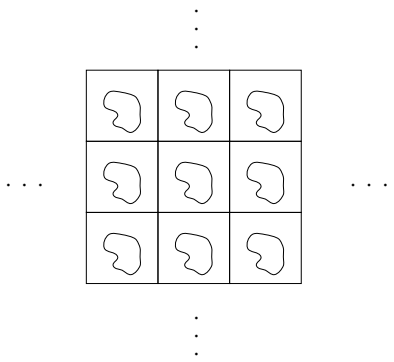

Figure 1: A square unit cell with a single inclusion and its eight nearest neighbors. The image cells extend in all directions.

and Λ the punctured lattice

$$\Lambda = \{k_1 + ik_2 \,|\, k_1, k_2 \in \boldsymbol{Z}, k_1^2 + k_2^2 \neq 0\}.$$

We proceed by replacing the kernels in the operators M_1 and M_2 by their periodic analogs. In other words, instead of the Cauchy kernel $1/(\tau - z)$ in eq. (9), we use the Weierstrass ζ function

$$\zeta(\tau, z) = \sum_{w \in \boldsymbol{Z}^2} \frac{1}{(w + \tau) - z}, \tag{14}$$

and instead of the kernel $(\tau - z)/(\bar{\tau} - \bar{z})^2$ in eq. (10), we use the function

$$\eta(\tau, z) = \sum_{w \in \boldsymbol{Z}^2} \frac{(w + \tau) - z}{((\bar{w} + \bar{\tau}) - \bar{z})^2}. \tag{15}$$

Rectangular and hexagonal arrays can be treated in an analogous fashion, as can skewed lattices in which the unit cell is an arbitrary parallelogram (Filshtinskii 1973).

Care must be taken in working with the functions $\zeta(\tau, z)$ and $\eta(\tau, z)$, since the series (14) and (15) are only conditionally convergent. To properly define these functions, we use the Taylor expansions

$$\zeta(\tau, z) = \left[\sum_{w \in \Lambda} \frac{1}{w}\right] + (z - \tau) \left[\sum_{w \in \Lambda} \frac{1}{w^2}\right] + (z - \tau)^2 \left[\sum_{w \in \Lambda} \frac{1}{w^3}\right] + \ldots \tag{16}$$

and

$$\begin{aligned} \eta(\tau, z) = \left[\sum_{w \in \Lambda} \frac{w}{\bar{w}^2}\right] + 2(\bar{z} - \bar{\tau}) \left[\sum_{w \in \Lambda} \frac{w}{\bar{w}^3}\right] + 3(\bar{z} - \bar{\tau})^2 \left[\sum_{w \in \Lambda} \frac{w}{\bar{w}^4}\right] + \ldots \\ + (z - \tau) \left[\sum_{w \in \Lambda} \frac{1}{\bar{w}^2}\right] + 2(z - \tau)(\bar{z} - \bar{\tau}) \left[\sum_{w \in \Lambda} \frac{1}{\bar{w}^3}\right] \\ + 3(z - \tau)^2(\bar{z} - \bar{\tau})^2 \left[\sum_{w \in \Lambda} \frac{1}{\bar{w}^4}\right] + \ldots \end{aligned} \tag{17}$$

The lattice sums which appear in these expressions are usually abbreviated by

$$S_j = \sum_{w \in \Lambda} \frac{1}{w^j}, \qquad j \geq 1,$$

and

$$T_j = \sum_{w \in \Lambda} \frac{w}{\bar{w}^{j-1}}, \qquad j \geq 3.$$

S_1 and T_3 can simply be set to zero, while S_j, for $j \geq 3$, and T_j, for $j \geq 5$, are convergent. The conditionally convergent sums S_2 and T_4 are "shape-dependent", with values determined by the condition that $\partial\zeta/\partial z$ and $\partial\eta/\partial z$ be periodic. For the square array, S_2 should be set to π, while T_4 is approximately 4.07845116116140 (Rayleigh 1892; Drummond and Tahir 1984). For an efficient algorithm to compute the convergent lattice sums, see Berman and Greengard (1994).

Once the periodic counterpart of eq. (8) has been solved for the density ω, the displacement field can be computed from eq. (2). Two useful functions related to the displacement are $p = \kappa(u + iv)$ and $q = \mu(u + iv)$. The functions p and q suffer from discontinuities (jumps) across inclusion/filler boundaries. The magnitudes of the jumps, the inside limit minus the outside limit, will be denoted $[p]$ and $[q]$. A straightforward calculation shows that

$$[q] = \left(1 + \frac{\mu_2}{2\kappa_2} + \frac{\mu_1}{2\kappa_1}\right)\omega(z) + \left(\frac{\mu_2}{\kappa_2} - \frac{\mu_1}{\kappa_1}\right) M_1\omega(z) + \left(\frac{\mu_2}{\kappa_2} - \frac{\mu_1}{\kappa_1}\right)\alpha z, \tag{18}$$

and that

$$[p] = \left(1 + \frac{\kappa_2}{2\mu_2} + \frac{\kappa_1}{2\mu_1}\right)\omega(z) + \left(\frac{\kappa_2}{2\mu_2} - \frac{\kappa_1}{2\mu_1}\right) M_2\omega(z) - \left(\frac{\kappa_2}{2\mu_2} - \frac{\kappa_1}{2\mu_1}\right)\bar{\beta}\bar{z}. \tag{19}$$

Repeated use of the divergence theorem yields

Lemma 3.1 *Let σ_{ij} and ϵ_{ij} denote the components of the stress and strain tensors, respectively, and let the stress-strain relations be given by*

$$\begin{pmatrix} \sigma_{11} \\ \sigma_{22} \\ \sqrt{2}\sigma_{12} \end{pmatrix} = \begin{pmatrix} c_1 & c_2 & c_3 \\ c_2 & c_4 & c_5 \\ c_3 & c_5 & c_6 \end{pmatrix} \begin{pmatrix} \epsilon_{11} \\ \epsilon_{22} \\ \sqrt{2}\epsilon_{12} \end{pmatrix}. \tag{20}$$

Let

$$a = \frac{1}{V}\int_{\Gamma_{\text{unit}}} [q]\mathrm{d}z \qquad \text{and} \qquad b = \frac{1}{V}\int_{\Gamma_{\text{unit}}} [p]\mathrm{d}\bar{z}, \tag{21}$$

where Γ_{unit} denotes the inclusion/filler interface in the unit cell. If one imposes the average displacement d_{I}, then the effective moduli c_{*1}, c_{*2}, c_{*3} are given by

$$\begin{aligned} c_{*1} &= \kappa_1 + \mu_1 + \Im\mathrm{m}\{a - b\}, \\ c_{*2} &= \kappa_1 - \mu_1 - \Im\mathrm{m}\{a + b\}, \\ c_{*3} &= -\sqrt{2}\Re\mathrm{e}\{a\}. \end{aligned} \tag{22}$$

If one imposes the average displacement d_{II}, then the effective moduli c_{*2}, c_{*4}, c_{*5} are given by

$$\begin{aligned} c_{*2} &= \kappa_1 - \mu_1 + \Im\mathrm{m}\{a - b\}, \\ c_{*4} &= \kappa_1 + \mu_1 - \Im\mathrm{m}\{a + b\}, \\ c_{*5} &= -\sqrt{2}\Re\mathrm{e}\{a\}. \end{aligned} \tag{23}$$

If one imposes the average displacement d_{III}, then the effective moduli c_{*3}, c_{*5}, c_{*6} are given by

$$\begin{aligned} c_{*3} &= \Im\mathrm{m}\{a - b\}/\sqrt{2}, \\ c_{*5} &= -\Im\mathrm{m}\{a + b\}/\sqrt{2}, \\ c_{*6} &= 2\mu_1 - \Re\mathrm{e}\{a\}. \end{aligned} \tag{24}$$

A useful formula, due to Hill (1964), applies to the case $\mu_1 = \mu_2$. The effective bulk modulus $\kappa_{\mathrm{eff}} = (c_{*1} + c_{*2})/2$ can then be written in closed form as

$$\kappa_{\mathrm{eff}} = \kappa_1 + \frac{(\mu_1 + \kappa_1)(\kappa_2 - \kappa_1)p_2}{\kappa_2 + \mu_1 - (\kappa_2 - \kappa_1)p_2}. \tag{25}$$

4 Numerical Preliminaries

One of the difficulties in working with integral equations is that they typically involve singular or weakly singular kernels. Initial inspection of the representations (9) and (10) would suggest that both M_1 and M_2 are singular, but they are not. The kernel of M_2 satisfies

$$\lim_{\tau \to z} \mathrm{d}\left[\log \frac{\tau - z}{\bar{\tau} - \bar{z}}\right] = \frac{1}{2}\kappa(z)ds, \tag{26}$$

and

$$\lim_{\tau \to z} \mathrm{d}\left[\frac{\tau - z}{\bar{\tau} - \bar{z}}\right] = \frac{1}{2}\kappa(z)e^{2i\theta}ds, \tag{27}$$

where $z(s)$ is a parameterization of the interface, $\kappa(z)$ denotes the curvature at the point $z(s)$, θ is the argument of the tangent vector at $z(s)$, and ds is an element of arclength. Thus, the kernel is continuous, at least for twice-differentiable curves. M_1, on the other hand, is a Cauchy integral, and must be interpreted in the principal value sense.

4.1 Fourier discretization

If the inclusions are disk-shaped, a very simple quadrature approach is to expand the density on each inclusion Γ_j as a Fourier series:

$$\omega_j(z) = \sum_{n=1}^{\infty} c_n^j e^{in\phi} + d_n^j e^{-in\phi}, \tag{28}$$

where ϕ denotes the argument of z with respect to the center of the jth disk. All of the integrals in eq. (8) can then be computed analytically, so that the only discretization error comes from truncating the Fourier representation (28).

4.2 The trapezoidal rule

For more general inclusions, the trapezoidal rule is commonly used with an equispaced mesh, since it achieves spectral accuracy when applied to smooth functions such as the integrand in $M_2\omega(z)$. If the point z lies on the interface Γ_j, then the Cauchy integral $M_1\omega(z)$ over $\Gamma - \Gamma_j$ can also be computed with spectral accuracy using the trapezoidal rule. It remains only to consider the evaluation of

$$M_1\omega_j(z) \equiv \frac{1}{2\pi i}\int_{\Gamma_j} \frac{\omega_j(\tau)\mathrm{d}\tau}{\tau - z}. \tag{29}$$

For this, we assume the number of points used in the discretization of Γ_j is even. It can then be shown that the trapezoidal rule using the odd points yields spectral accuracy at the even points, and vice versa (Sidi and Israeli 1988).

If distinct portions of the total interface Γ are relatively well separated, then the method just outlined works extremely well. This condition can be violated by a single inclusion whose boundary folds back on itself, or by having two inclusions be close to touching. In either event, the trapezoidal rule performs poorly. If the underlying mesh has a spacing of h, it requires that distinct, non-adjacent portions of the boundary be relatively far away (perhaps $10h$) in order for the integrand to appear smooth, even if the density ω is well-resolved.

4.3 Product integration

Boundary element methods (Jaswon and Symm 1977) are based on product integration, and are not plagued by the same difficulty. To achieve uniform second order accuracy, for example, the density ω would be approximated by a piecewise linear function and the interface by a polygon. All integrals would then be evaluated analytically. Such a technique is viable, but we have chosen to use adaptive Gaussian quadrature because it is easy to implement, it is easy to refine locally, and it provides us with robust *a posteriori* error control.

4.4 Adaptive Gaussian quadrature

Suppose that the boundary Γ is subdivided into M segments, and that on each segment we are given the nodes corresponding to K-point Gauss-Legendre quadrature in the arclength parametrization as well as the values of ω at those nodes. Then, for smooth integrands, the composite K-point rule is of order $2K$. Thus, if distinct portions of the boundary are not close-to-touching, the application of the operator M_2 is straightforward. If the point z lies on the interface Γ_j, then the Cauchy integral $M_1\omega(z)$ over $\Gamma - \Gamma_j$ is also computed with $2K$th order accuracy. For the calculation of $M_1\omega_j(z)$, we assume that Γ_j is parametrized in arclength as $\Gamma_j = \{\tau(s) \,|\, 0 \le s \le |\Gamma_j|\}$, and let $z = \tau(t)$. We write $M_1\omega_j(z)$ in the form

$$M_1\omega_j(\tau(t)) = \frac{\omega_j(\tau(t))}{2} + \frac{1}{2\pi i}\int_{\Gamma_j} \frac{(\omega_j(s) - \omega_j(t))\tau'(s)\,ds}{\tau(s) - \tau(t)}. \tag{30}$$

Since

$$\lim_{s\to t} \frac{\omega_j(s) - \omega_j(t)}{\tau(s) - \tau(t)} = \frac{\omega_j'(t)}{\tau'(t)},$$

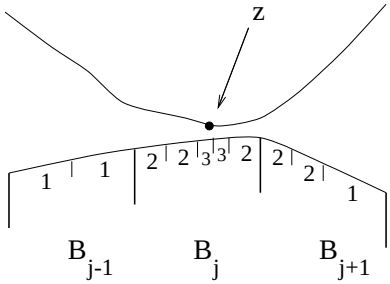

Figure 2: For points such as z, adaptive Gaussian quadrature is used to evaluate the integrals $M_1\omega(z)$ and $M_2\omega(z)$ over the three nearby segments B_{j-1}, B_j, and B_{j+1}. All three are refined once, several subintervals are refined a second time, and one is refined a third time (indicated by the numbers 1,2,3).

the integral in (30) has a smooth kernel. The derivatives $\omega'(t)$ and $\tau'(t)$ can, of course, be computed with Kth order accuracy using the values of ω and τ at the K nodes on a given segment. Therefore, the Cauchy principal value integral can be obtained with Kth order (but not $2K$th order) accuracy.

If distinct, non-adjacent portions of the interface Γ are close-to-touching, then we encounter the same difficulty as we did with the trapezoidal rule. To overcome this, we use a strategy devised and discussed in some detail by Helsing (1996) in the context of electrostatic problems. For illustration, consider the evaluation of $M_1\omega(z)$, where z is near, but not on, three consecutive segments B_{j-1}, B_j, B_{j+1} in the discretization of Γ. We assume that other segments are sufficiently far that the kernel $\mathrm{d}\tau/(\tau - z)$ appears smooth (Fig. 2). To compute

$$\frac{1}{2\pi i}\int_{B_{j-1}} \frac{\omega(\tau)\mathrm{d}\tau}{\tau - z}, \quad \frac{1}{2\pi i}\int_{B_j} \frac{\omega(\tau)\mathrm{d}\tau}{\tau - z}, \quad \text{and } \frac{1}{2\pi i}\int_{B_{j+1}} \frac{\omega(\tau)\mathrm{d}\tau}{\tau - z},$$

we use recursive binary subdivision of each interval. The refinement process is halted when the kernel $\mathrm{d}\tau/(\tau - z)$ is sufficiently well resolved by a K-point Gauss-Legendre mesh. The density ω is then interpolated to the points of the refined mesh and the integral is evaluated by (composite) Gauss-Legendre quadrature. To be more precise about this decision process, we use a heuristic rule based on examining the Legendre expansion of the kernel as a function of arclength s:

$$\frac{|S_\Gamma|\tau'(s)}{\tau(s) - z} \approx \sum_{k=0}^{K-1} c_k P_k(s),$$

where $P_k(s)$ is the kth order Legendre polynomial scaled to the relevant subinterval and $|S_\Gamma|$ is the length of that subinterval. Smoothness is then well-known to correspond to rapid decay of the coefficients $\{c_k\}$ (Gottlieb and Orszag 1977). We halt the refinement process when $|c_{K-2}| + |c_{K-1}| < \sqrt{\epsilon}$, where ϵ is the desired precision. We use $\sqrt{\epsilon}$ rather than ϵ as our "monitor function" because the approximation of the kernel is only Kth order accurate, while the quadrature rule is of order $2K$.

Remark 4.1 When solving the discrete version of the integral equation (8), what is needed is only the influence of each density value ω_j at each discretization point z_k. The adaptive

calculation need only be done once to obtain the corresponding matrix entry accurately. The adaptive refinement strategy outlined above does *not* increase the number of degrees of freedom.

4.4.1 *A posteriori* refinement

One of the principal advantages of using composite Gaussian quadrature is that it provides an extremely reliable form of error control. After solving the integral equation (8) on a given subdivision of Γ, we can expand the solution ω on each segment and determine whether it is well-resolved by looking at its Legendre expansion. Those subintervals on which ω is rapidly decaying can then be left untouched, while those on which the decay is slow can be subdivided, after which the full integral equation must be solved again. A reasonable strategy is to use a similar refinement criterion as above, namely that $|c_{K-2}| + |c_{K-1}| < \epsilon$. We modify this approach by fixing the number of subdivisions added at each stage and allowing multiple subdivisions of a given interval, if deemed appropriate. We refer the reader to (Helsing 1996) for details. Given an initial subdivision structure for Γ, we refer the process of solving the integral equation and refining underresolved segments as a *stage*. For a discussion of why such a strategy is particularly robust in an integral equation framework, see (Lee and Greengard 1997).

4.5 Fast multipole acceleration

Discretization of the integral equation (8), or its periodic counterpart, results in a dense linear system, for which $O(N^2)$ work is required to generate the matrix. When the number of unknowns is sufficiently small, direct elimination schemes can be used to solve these systems with a cost proportional to N^3. Since the linear systems are well-conditioned, however, conjugate-gradient type iterative methods such as GMRES or BCG require the evaluation of a fixed number of matrix-vector products which depends on the error tolerance, but is independent of N. Thus, good iterative techniques require $O(N^2)$ work. The amount of work can be reduced to $O(N)$ by making use of the fast multipole method or FMM (Rokhlin 1985; Greengard and Rokhlin 1987; Carrier *et al.* 1988), which is a "matrix-free" approach. We refer the reader to these papers for a description of the method and to (Greenbaum, Greengard, and Mayo 1992; Greengard *et al.* 1996) for its use in related problems.

We have been rather loose in our lack of distinction between the infinite medium problem and the periodic problem. As noted in section 3, the transition from the infinite medium problem to the periodic problem is easily made by the addition of certain lattice sums to each matrix entry. One of the features of the FMM is that periodic boundary conditions are easy to incorporate. We refer the reader to (Greengard and Rokhlin 1987; Berman and Greengard 1994) for details.

5 Results

The method described above for the periodic problem has been implemented in Fortran. To analyze its performance, we have tested it on inclusion problems with a variety of geometries.

Table 1: Effective elastic moduli for square arrays of disks with elastic moduli $\mu_2 = 135$ and $\kappa_2 = 225$ embedded in a filler with moduli $\mu_1 = 1$ and $\kappa_1 = 3\frac{1}{3}$. p_2 denotes the area fraction of the disks. The effective bulk modulus is $\kappa_{\text{eff}} = (c_{*1} + c_{*2})/2$ and the effective shear moduli are $\mu^1_{\text{eff}} = (c_{*1} - c_{*2})/2$ and $\mu^2_{\text{eff}} = c_{*6}/2$. N_{Fourier} denotes the number of modes needed in the Fourier discretization to obtain the moduli to the number of digits shown, while N_{trap} denotes the number of points needed in the trapzoidal discretization.

p_2	N_{Fourier}	N_{trap}	κ_{eff}	μ^1_{eff}	μ^2_{eff}
0.1	6	22	3.8045847395	1.1971387003	1.1625163756
0.2	8	28	4.3910679595	1.4924686151	1.3373951533
0.3	8	36	5.1425863254	1.9415606008	1.5410983175
0.4	10	52	6.1476105376	2.6433812382	1.8013994273
0.5	12	76	7.5905993679	3.7984374034	2.1743265379
0.6	16	140	9.9699203299	5.9094871031	2.8031074855
0.7	24	300	15.4285904402	10.9105341255	4.2840181567
0.78	94	6000	44.0056413856	33.0679995249	14.6242590661
0.785	300	-	57.7483590340	41.5392409243	27.277092151
0.78539	1000	-	59.7403738343	42.6712066524	32.46299651

Example 1: Periodic arrays of disks

We first consider periodic arrays of disks using both Fourier discretization and the trapezoidal rule. In order to compare our results with previous calculations (Lukkassen *et al.* 1995), we have selected the component moduli to be $\kappa_1 = 4.3$, $\mu_1 = 1.3$, $\kappa_2 = 48.6$, and $\mu_2 = 29.2$, with disk area fraction equal to 0.45. Only twenty nonzero Fourier coefficients are needed to obtain $c_{*1} = 11.69212100848$, $c_{*2} = 4.423994909931$ and $c_{*6}/2 = 2.458447333489$. Lukkassen *et al.* (1995) obtained effective moduli $c_{*1} = 11.7$, $c_{*2} = 4.5$, and $c_{*6}/2 = 2.4$. In Table 1, we provide the effective moduli for square arrays of elastic disks over a wide range of area fractions for greater material contrast. As the inclusions begin to approach their neighboring images, the number of Fourier modes grows noticeably, but the difficulties encountered by the trapezoidal rule are more severe. For area fractions above $p_2 = 0.78$, several thousand points are required to compute the integrals $M_1\omega(z)$ and $M_2\omega(z)$ with a single digit of accuracy.

Example 2: A single complex inclusion

Figure 3 shows a square array of nine-armed inclusions. The interface of the inclusion in the unit cell centered at the origin is parameterized by

$$z(t) = 0.36(1 + 0.36\cos 9t)e^{it}, \qquad 0 \le t < 2\pi. \tag{31}$$

Using the same component moduli as in Table 1, we obtain $c_{*1} = 13.00586195521$, $c_{*2} =$

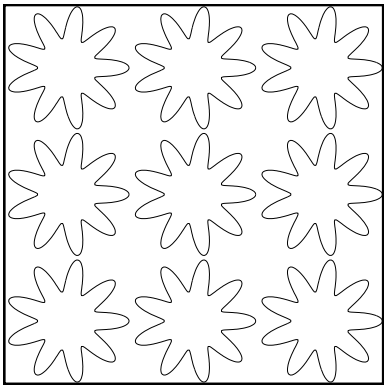

Figure 3: A unit cell and its nearest neighbors in an array of nine-armed inclusions, parametrized as in eq. (31).

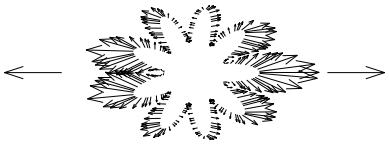

Figure 4: For stretching in the x-direction (displacement d_{I}), we plot the traction vector along the inclusion/filler interface.

3.629623366442, $c_{*4} = 15.06532778649$, and $c_{*6} = 5.51963404857$, using either the composite 24-point Gauss-Legendre rule or the trapezoidal rule for discretization. We also display the traction along the interface in Fig. 4. It is interesting to note that for twelve digit accuracy, Gauss-Legendre quadrature is slightly more efficient, requiring 1200 points on the interface where the trapezoidal rule required 1300 points. Using a Sun Ultra workstation, the setup time required to generate and store the matrices corresponding to the operators M_1 and M_2 is less than two minutes. The subsequent solution time for each of the three right-hand sides is approximately two and a half minutes using the iterative method GMRES.

Examples 3,4: Thin bridges

We next consider single inclusions whose interface creates thin bridges (close-to-touching areas). For this, we use the adaptive Gaussian quadrature method of section 4. These problems are still of modest size, and we continue to generate and store the full matrices corresponding to the operators M_1 and M_2. The system of linear equations resulting from eq. (8) is then solved with BCG iteration. For accuracies on the order of ten digits, we have found 16-point Gauss-Legendre quadrature to be most efficient, and use that in the remainder of this paper.

Remark 5.1 For the sake of comparison, we first apply the adaptive method to the square array of disks at area fraction $p_2 = 0.78539$. With 256 discretization points we obtain four to five accurate digits in the effective moduli κ_{eff}, μ^1_{eff} and μ^2_{eff}. After three stages of

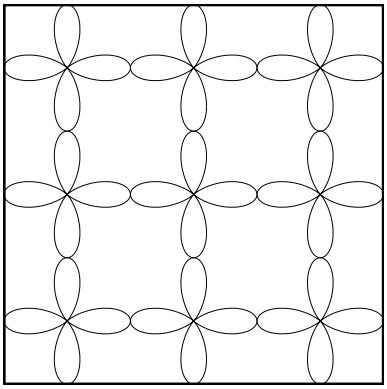

Figure 5: A unit cell and its nearest neighbors in an array of inclusions, parametrized as in eq. (32).

Table 2: Effective elastic moduli for Example 3 (Fig. 5). The component elastic moduli are the same as for Example 1. The first column indicates the stage of refinement, the effective moduli are defined as in Table 1. N is the number of discretization points, 'Iter' is the total number of BCG iterations for the two sets of equation that are solved at each stage, and 'Time' is the total elapsed computing time in minutes on a SUN Sparc10 workstation.

Stage	κ_{eff}	μ^1_{eff}	μ^2_{eff}	N	Iter	Time
1	15.9	11.1	1.64	256	141	1m
2	15.93	11.13	1.640	512	172	6m
4	15.934	11.128	1.6396	1024	195	40m
6	15.93429	11.12822	1.639619	1152	188	97m
8	15.9342890	11.1282176	1.63961932	1408	78	152m

refinement, 896 discretization points are introduced and the effective moduli are obtained with better than ten digit accuracy.

Our third example is depicted in Fig 5, parameterized in the unit cell by

$$z(t) = 0.25(1 + 0.999\cos 4t)e^{it}, \qquad 0 \le t < 2\pi. \tag{32}$$

The area fraction of the inclusion is $p_2 = \pi(2 + 0.999^2)/16$. As a test of accuracy, we first choose $\mu_1 = \mu_2 = \kappa_1 = 1$ and $\kappa_2 = 1000$, and test our results against Hill's formula (25). The exact effective bulk modulus should be $\kappa_{\text{eff}} = 1.8318182778838$, and the program gives $\kappa_{\text{eff}} = 1.8318183$ at the first stage of refinement. In Table 2, we present the effective moduli when the components have the moduli of Example 1. We also show the time required as the calculation proceeds. The solution of the integral equation at the first stage of refinement requires one minute on a SUN Sparcstation 10. At the end of stage two, six minutes have elapsed, and at the end of stage eight, two and one half hours have elapsed.

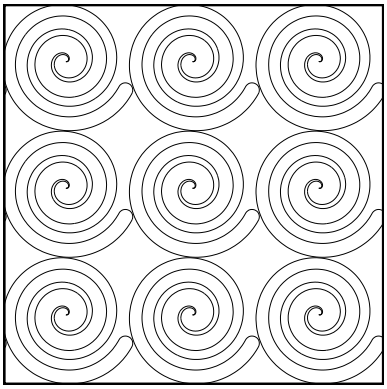

Figure 6: A unit cell and its nearest neighbors in an array of "rolls", parametrized as in eq. (33).

Table 3: Effective elastic moduli for the square array of rolls (Fig. 6). The component elastic moduli are as in Table 1. The first row shows the number N of points required.

	Stage 1	Stage 2	Stage 3	Stage 4	Stage 5
N	704	1008	1312	1552	1696
c_{*1}	17.95	18.0072144	18.00721389	18.0072138812	18.0072138809
c_{*2}	11.04	11.0658627	11.0658627	11.06586271	11.065862712
c_{*3}	1.9	1.948818	1.9488175	1.948817513	1.948817512
c_{*4}	16.712	16.7186922	16.71869263	16.718692679	16.7186926829
c_{*5}	1.17	1.16891	1.1689136	1.16891359	1.168913589
c_{*6}	9.03	9.0139564	9.01395633	9.013956306	9.0139563042

A third example is the array of "rolls" in Figure 6. A roll has the parameterization

$$z(t) = \begin{cases} 0.58te^{i6\pi t}e^{-i\pi/7} & 0 \le t < 1 \\ (0.522 - 0.058e^{i\pi t})e^{-i\pi/7} & 1 \le t < 2 \\ 0.464(3-t)e^{-i6\pi t}e^{-i\pi/7} & 2 \le t < 3 \end{cases} \tag{33}$$

It is interesting to note that the close-to-touching points are well-resolved after only one stage of refinement. Subsequent stages of refinement take place primarily at the breakpoints $t = 0, 1, 2$ in the parametrization (33), which is continuous, but not smooth. The effective moduli are presented in Table 3.

Example 5: Eight elliptical inclusions

Figure 7 shows a suspension with eight equisized ellipses in the unit cell. The aspect ratio of their axes is 2:1 and their area fraction is $p_2 = 0.7$. Each ellipse interface has the parameterization

$$z(t) = z_{\text{cent}} + \sqrt{\frac{0.7}{16\pi}}e^{i\alpha}(2\cos t + i\sin t), \qquad -\pi \le t < \pi. \tag{34}$$

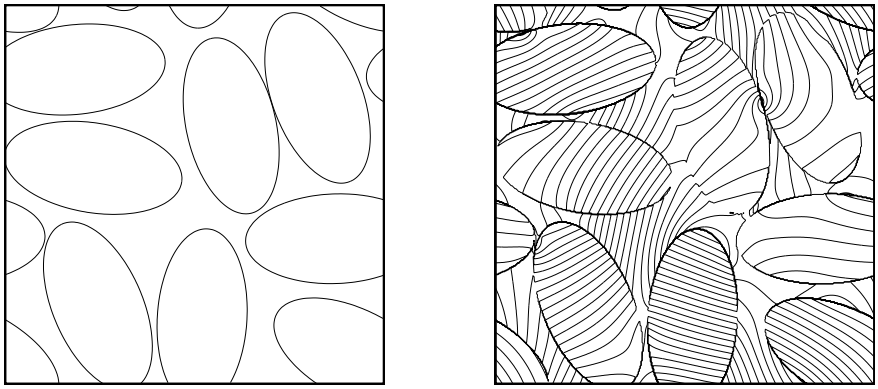

Figure 7: The left-hand image depicts a unit cell consisting of a suspension of eight ellipses with aspect ratio 2:1 at area fraction $p_2 = 0.7$. The right-hand picture is a contour plot of the trace of the stress tensor when the composite is subject to a balanced biaxial average displacement $(d_{\rm I} + d_{\rm II})/2$.

Table 4: Center coordinates $x_{\rm cent}$, $y_{\rm cent}$, and rotations α for the eight ellipses composite depicted in Figure 7.

ellipse no.	$x_{\rm cent}$	$y_{\rm cent}$	α
1	0.096558008044553	0.180606440983544	1.793069456776903
2	-0.312317331860957	0.328928705317157	0.103527236861962
3	0.020093822024223	-0.326279205482295	-1.631099491555291
4	0.426052439830122	-0.422860540089244	-0.473183135086323
5	0.323978421616729	0.254064864498771	-1.204877840652208
6	-0.266711719264471	0.070034693393812	-0.162392923788297
7	0.370486724007364	-0.116660224915378	0.034300608334877
8	-0.254250775518318	-0.294308693171502	1.979465648427812

The eight centers $z_{\rm cent}$ and rotations α are given in Table 4. The effective elastic moduli are presented in Table 5 as a simple, but nontrivial, benchmark for those interested in testing codes. The trace of the stress tensor, depicted in Fig. 7, is obtained from the standard formula (Muskhelishvili 1953; Parton and Perlin 1981)

$$\sigma_{11} + \sigma_{22} = 4\,\Re\mathrm{e}\left\{\phi'(z)\right\}.$$

Example 6: Random dispersions of disks

In the preceding examples the entries in the matrices corresponding to M_1 and M_2 are precomputed and stored – a practice whose cost in time and storage grows as N^2, where N is the number of discretization points on the interface Γ. For large-scale problems, we use the iterative solver GMRES with fast multipole acceleration, as discussed briefly in section 4.

Table 5: Effective elastic moduli for the suspension of ellipses Example 5. The component elastic moduli are as in Table 1. N denotes the number of discretization points used at each stage of refinement.

	stage 1	stage 2	stage 3
c_{*1}	22.527428	22.527424771	22.5274247710
c_{*2}	7.840472	7.840472273	7.8404722733
c_{*3}	-0.630457	-0.630456718	-0.6304567184
c_{*4}	21.216677	21.216677187	21.2166771874
c_{*5}	-1.483319	-1.483318320	-1.4833183202
c_{*6}	11.826784	11.826785793	11.8267857932
N	1280	1664	2048

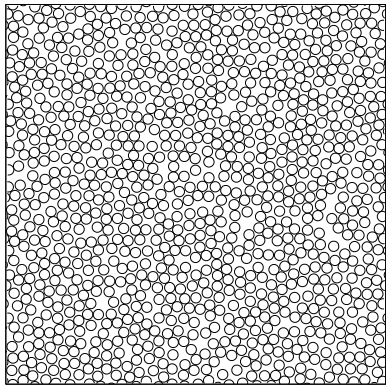

Figure 8: A unit cell with a "random" suspension of 1024 disks at area fraction $p_2 = 0.6$.

Table 6: Effective elastic moduli for the "random" suspension of 1024 disks in Figure 5. The component elastic moduli are as in Table 1. N denotes the number of discretization points used at each stage of refinement.

	Stage 1	Stage 2	Stage 3
c_{*1}	15.4	15.4020	15.40199076
c_{*2}	6.2	6.2333	6.23335354
c_{*3}	0.1	0.0592	0.05920050
c_{*4}	15.4	15.3804	15.38044155
c_{*5}	0.0	0.0285	0.02852952
c_{*6}	9.1	9.0653	9.06533520
N	131,072	163,840	196,608

Random suspensions of disks were generated with a Monte Carlo Technique (Metropolis, Rosenbluth, Rosenbluth, Teller, and Teller 1953). We began with a regular array and assigned random tentative displacements to all disks. Each disk was examined in turn. If its new position did not cause disks to overlap, the move was accepted. The mean size of the random displacements was chosen so that the probability of acceptance was 0.5. When *all* disks were examined once, we considered one simulation step to have been completed. One million simulation steps resulted in the configuration of Fig. 8. Eight segments and 131,072 points were used at the first stage of refinement, and 19 GMRES iterations were needed for each of the three right-hand sides to solve the system with a tolerance of 10^{-3}. The total time required on a SUN Ultra workstation was 2 hours. After two additional stages of refinement were completed, 28 hours had elapsed.

Example 7: Random dispersions of thin ellipses

We have also considered "random" dispersions of thin ellipses (Fig. 9), generated by a 200,000 step Monte Carlo procedure. In the solution process, 16 segments were initially placed on each ellipse. Four stages of refinement were used with 480 new segments added per stage. The computed effective moduli are presented in Table 7, along with timing results.

Example 8: Highly irregular inclusions

Our final example consists of four highly irregular inclusions in the unit cell (Fig. 10). In the solution process, 250 segments were initially placed on each inclusion and 200 new segments were added per stage. At stage 3, 140 GMRES iterations were needed with a tolerance of 10^{-14}, consuming about 5 hours of time on a SUN Ultra workstation. The effective moduli are presented in Table 8.

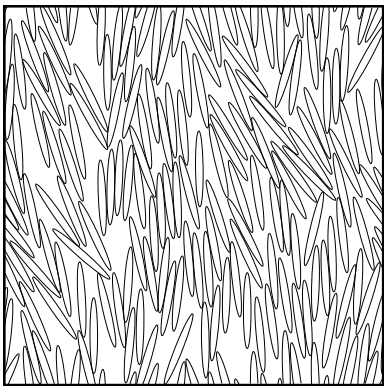

Figure 9: A unit cell with a "random" suspension of 160 ellipses with aspect ratio 10:1 at area fraction $p_2 = 0.5$.

Table 7: Effective elastic moduli for the "random" suspension of 160 ellipses in Figure 6. The component elastic moduli are the same as in Table 1. N denotes the number of discretization points used at each stage of refinement, 'Iter' denotes the number of GMRES iterations required for the accuracies displayed, and 'Time' denotes the number of hours required on a SUN Ultra workstation to solve all three interface problems, corresponding to displacements d_{I}, d_{II}, and d_{III}.

	Stage 1	Stage 2	Stage 3	Stage 4
c_{*1}	9.3024	9.3023926	9.3023925873	9.3023925873
c_{*2}	5.9947	5.9949691	5.9949691278	5.9949691278
c_{*3}	-0.7498	-0.7497692	-0.7497692321	-0.7497692320
c_{*4}	29.4173	29.4198727	29.4198730363	29.4198730364
c_{*5}	-3.3983	-3.3979440	-3.3979439966	-3.3979439966
c_{*6}	7.5263	7.5263686	7.5263686500	7.5263686499
N	40,960	48,640	56,320	64,000
Iter	50	91	120	120
Time	3 hrs	8 hrs	13 hrs	16 hrs

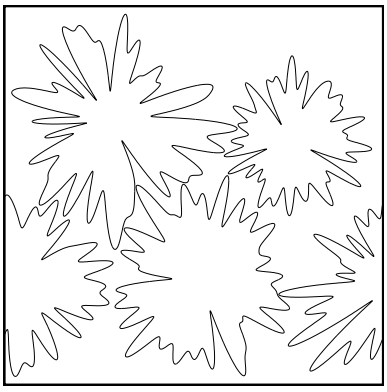

Figure 10: A unit cell with four irregular inclusions at area fraction $p_2 = 0.463$.

Table 8: Effective elastic moduli for the irregular inclusions of Example 8 (Fig. 10). The component elastic moduli are the same as in Table 1. N denote the number of discretization points used at each stage of refinement.

	Stage 1	Stage 2	Stage 3
c_{*1}	17.294	17.294395704	17.294395704665
c_{*2}	5.072	5.071676773	5.071676772940
c_{*3}	-0.006	-0.006236690	-0.006236690506
c_{*4}	12.880	12.879949658	12.879949658049
c_{*5}	0.057	0.057492106	0.057492106002
c_{*6}	6.605	6.604769982	6.604769981583
N	22,400	25,600	28,800

6 Conclusions

We have developed a fast, adaptive and high-order solver for locally isotropic problems of planar elasticity. The algorithm has an extremely simple user interface, requiring only the location of the inclusion boundaries and the elastic moduli of the components. Complex grid generation is avoided, and the adaptive refinement of close-to-touching areas is automatic.

The scheme can be extended in a straightforward way to biconnected composites and to crack problems. We are also considering three-dimensional problems, for which a suitable potential theory can be found, for example, in (Parton and Perlin 1981).

References

Achenbach, J. D. and Zhu, H. (1990), Effect of interphases on micro and macromechanical behavior of hexagonal-array fiber-composites, *J. Appl. Mech.* **57**, 956-963.

Berman, C. L., and Greengard, L. (1994), A Renormalization Method for the Evaluation of Lattice Sums, *J. Math. Phys.* **35**, 6036-6048.

Carrier, J., Greengard, L., and Rokhlin, V. (1988), A fast adaptive multipole algorithm for particle simulations, *SIAM J. Sci. and Stat. Comput.* **9**, 669-686.

Chen, J., Thorpe, M. F., and Davis, L. C. (1995), Elastic properties of rigid fiber-reinforced composites, *J. Appl. Phys.* **77**, 4349-4360.

Drummond, J. E. and Tahir, M. I. (1984), Laminar viscous flow through regular arrays of parallel solid cylinders, *Int. J. Multiphase Flow* **10**, 515-540.

Eischen, J. W. and Torquato, S. (1993), Determining elastic behavior of composites by the boundary element method, *J. Appl. Phys.* **74**, 159-170.

Filshtinskii, L. A. (1973), On the theory of elastic nonhomogeneous meida with a regular structure, *PMM* **37**, 262-273.

Fletcher, R. (1975), Conjugate gradient methods for indefinite systems, in *Proc. of the Dundee Biennial Conference on Numerical Analysis*, G. A. Watson, ed., Springer-Verlag, New York.

Garboczi, E. J., and Day, A. R. (1995), An algorithm for computing the effective linear properties of heterogeneous materials, *J. Mech. Phys. Solids*, **43**, 1349-1362.

Greenbaum, A., Greengard, L. and Mayo, A. (1992), On the numerical solution of the biharmonic equation in the plane, *Physica D* **60**, 216-225.

Greengard, L., Kropinski, M. C., and Mayo, A. (1996), Integral equation methods for Stokes flow and isotropic elasticity in the plane, *J. Comput. Phys.* **125**, 403-414.

Greengard, L. and Moura, M. (1994), On the numerical evaluation of electrostatic fields in composite materials, *Acta Numerica*, 379-410.

Greengard, L. and Rokhlin, V. (1987), A fast algorithm for particle simulations, *J. Comput. Phys.* **73**, 325-348.

D. Gottlieb and S. Orszag (1977), *Numerical Analysis of Spectral Methods*, SIAM, Philadelphia, Penn.

Helsing, J. (1995), An integral equation method for elastostatics of periodic composites, *J. Mech. Phys. Solids* **43**, 815-828.

Helsing, J. (1996), Thin bridges in isotropic electrostatics, *J. Comput. Phys.* **127**, 142-151.

Hill, R. (1964), Theory of mechanical properties of fibre-strengthened materials: I. elastic behaviour, *J. Mech. Phys. Solids* **12**, 199-212.

Honein, T. and Herrmann, G. (1990), On bonded inclusions with circular or straight boundaries in plane elastostatics, *J. Appl. Mech* **57**, 850-856.

Jaswon, M. A. and Symm, G. T. (1977), *Integral Equation Methods in Potential Theory and Elastostatics*, Academic Press, New York.

Jou, H.-J., Leo, P. H., and Lowengrub, J. S. (1995), Microstructural evolution in inhomogeneous elastic media, *University of Minnesota Supercomputing Institute Research Report UMSI 95/177*

Lanczos, C. (1952), Solution of systems of linear equations by minimied iteration, *J. Res. Nat. Bur. Standards* **49**, 33-53.

Lee, J.-Y. and Greengard, L. (1997), A fast adaptive numerical method for two-point boundary value problems, *SIAM J. Sci. Comput.*, to appear.

Lukkassen, D., Persson, L.E. and Wall, P. (1995), Some engineering and mathematical aspects of the homogenization method, *Composites Engineering* **5** 519-531.

Metropolis, N., Rosenbluth, A. W., Rosenbluth, M. N., Teller, A. N., and Teller, E. (1953), Equation of state calculations by fast computing machines, *J. Chem. Phys.* **21**, 1087-1092.

McPhedran, R. C. and Movchan, A. B. (1994), The Rayleigh multipole method for linear elasticity, *J. Mech. Phys. Solids* **42**, 711-727.

Mura, T. (1987), *Micromechanics of Defects in Solids*, Martinus Nijhoff Publishers, Dordrecht.

Muskhelishvili, S. G. (1953), *Some Basic Problems of the Mathematical Theory of Elasticity*, P. Noordhoff Ltd, Groningen.

Parton, V. Z. and Perlin, P. I. (1982), *Integral Equation Methods in Elasticity*, MIR, Moscow.

J. W. Rayleigh (1892), On the influence of obstacles arranged in rectangular order upon the properties of a medium, *Phil. Mag.* **34**, 481-502.

Rokhlin, V. (1985), Rapid solution of integral equations of classical potential theory, *J. Comput. Phys.* **60**, 187-207.

Y. Saad and M. H. Schultz (1986), GMRES: a generalized minimum residual algorithm for solving nonsymmetric linear systems, *SIAM J. Sci. Stat. Comput.* **7**, 856-869.

Sherman, D. I. (1959), On the problem of plane strain in non-homogeneous media, in *Non-homogeneity in Elasticity and Plasticity*, W. Olszak, ed., Pergamon Press, 3-20.

A. Sidi and M. Israeli (1988), Quadrature methods for periodic singular and weakly singular Fredholm integral equations, *J. Sci. Comput.* **3**, 201-231.

Theocaris, P. S. and Ioakimidis, N. I. (1977), The inclusion problem in plane elasticity, *Q. J. Mech. Appl. Math.* **30**, 437-448.